Rh, Ru and Pt ternary perovskites type oxides $BaZr_{(1-x)}Me_xO_3$ for methane dry reforming

Benedetta de Caprariis[a], Paolo De Filippis[a,*], Vincenzo Palma[b], Antonietta Petrullo[a], Antonio Ricca[b], Concetta Ruocco[b], Marco Scarsella[a]

a *Department of Chemical Engineering, Sapienza University of Rome, Via Eudossiana 18, Rome, Italy.*

b *Department of Industrial Engineering, University of Salerno, Via Giovanni Paolo II, 132, Fisciano (SA), Italy.*

Corrisponding author: paolo.defilippis@uniroma1.it Tel: +390644585562

Abstract

In recent years dry reforming of methane has received considerable attention as a promising alternative to steam reforming for synthesis gas (H_2 and CO) production, yielding a syngas with a H_2/CO ratio close to 1 and thus suitable for many chemical processes. The major drawback of the process is the endothermicity of the reaction that implies the use of a suitable catalyst to work at relatively low temperatures (923-1023 K). In this work methane dry reforming over three ternary perovskite type oxides $BaZr_{(1-x)}Me_xO_3$ using Rh, Ru and Pt as metal was studied at atmospheric pressure and in a temperature range 850–1150 K. Experimental tests at different temperatures were performed in order to analyze and compare the performances of the catalysts and to carry out a detailed kinetic study. Furthermore, long duration tests were conducted to evaluate the possible deactivation of the perovskites.
Rhodium-perovskite catalyst shows the highest activity for dry methane reforming while the Pt one the lowest. No deactivation of the catalysts was observed meaning that the perovskite structure is very stable and allows to minimize the carbon deposition that is the main responsible of catalyst deactivation in this process.

1. Introduction

In recent years CO_2 (dry) reforming of hydrocarbons such as methane (DRM) has received considerable attention as a promising alternative to steam reforming for synthesis gas (H_2 and CO) production [1-5].
This process could be industrially advantageous, yielding a syngas with a H_2/CO ratio close to 1, suitable for Fischer-Tropsch synthesis to liquid hydrocarbons and for the production of valuable oxygenated chemicals [1, 5-8]. DRM features also some potential environmental implications, utilizing the main greenhouse effect contributors (CH_4 and CO_2) and transforming them into high added value products.
Furthermore DRM allows the direct utilization of renewable feedstock as biogas from various anaerobic biological waste processes for syngas or hydrogen production [9, 10].
The major drawbacks are related to the high endothermic nature of the dry reforming reaction (1)

$$CH_4 + CO_2 \leftrightarrow 2CO + 2H_2 \qquad \Delta H^0_{298K} = 247\ kJmol^{-1} \qquad (1)$$

and to the concurring side reactions, the most important of which are the reverse water–gas shift reaction (RWGS) (2), the methane cracking reaction (3) and the Boudouard reaction (4)

$CO_2 + H_2 \leftrightarrow CO + H_2O$ $\Delta H^0_{298K} = 41\ kJmol^{-1}$ (2)

$CH_4 \leftrightarrow C + 2H_2$ $\Delta H^0_{298K} = 75\ kJmol^{-1}$ (3)

$2CO \leftrightarrow C + CO_2$ $\Delta H^0_{298K} = -171\ kJmol^{-1}$ (4)

The extent of these competitive reactions influences the selectivity of the DRM process, modifying the CH_4 and CO_2 equilibrium conversions. Moreover formation of carbon takes place from both reactions (3) and (4), being reaction (4) favoured at temperatures below 973 K and reaction (3) at higher temperatures. The consequent deactivation of DRM catalysts due to the carbon deposition constitutes a serious limit in the industrial DRM reaction development [1].
Thus, for achieving industrially relevant conversions at relatively moderate temperatures, the use of a catalyst with high activity and selectivity for the DRM reaction and with good stability towards carbon deposition is required.
Supported metals of groups 8, 9 and 10 are known to be active and stable catalysts for the DRM reaction, the order of activity for these metals being Ru ~ Rh > Ni ~ Ir > Pt > Pd [11].
Perovskite-type oxides (ABO_3, where A = alkali, alkaline earth or rare-earth elements and B = transition metal) as precursors in the catalytic DRM are receiving growing attention. These oxides show high thermal and hydrothermal stability and when subjected to reduction of the B-site cations they produce nanometric particles with the transition metal highly dispersed at the surface of the basic support [12,13], thus increasing the catalytic activity and stability and providing unfavourable conditions to carbon deposition. Moreover the catalytic performances can be strongly affected by the partial substitution at A and B sites, modifying the transition metal oxidation state, the oxygen mobility within the crystal lattice and the catalyst redox properties [14-16].
In this work, a series of ternary perovskite type oxides $BaZr_{(1-x)}Me_xO_3$ (Me= Rh, Ru, Pt) were prepared using a variant of the citrate method [17] starting from the ideal cubic $BaZrO_3$ perovskite structure that shows excellent thermal stability and resistance in the typical DRM temperature range thanks to its low coefficient of thermal expansion [18,19] and partially substituting the B-site zirconium with the catalytically active transition metals. The catalytic properties of the so obtained oxides were tested at different temperatures. Long duration experiments were performed in order to evaluate the resistance of the catalysts to carbon deposition. Finally the kinetic parameters were calculated from the tests conducted at different temperature using the model of Wei and Iglesia [20].

2. Experimental section

2.1 Synthesis of perovskite type oxides

Three ternary perovskite type oxides were prepared using a variant of the citrate method [17] to obtain the precursors for the catalytic DRM containing a percentage of active metal respectively of 5% for rhodium ($BaZr_{0.8649}Rh_{0.1351}O_3$), ruthenium ($BaZr_{0.8649}Ru_{0.1351}O_3$) and platinum ($BaZr_{0.9272}Pt_{0.0728}O_3$).
A solution of citric acid (Carlo Erba) was added under continuous stirring to a water suspension of the zirconium precursor (zirconium isopropoxide, Aldrich) and the mixture was kept at its boiling point for 4 hours in order to assure the complete solubilization of zirconium. After cooling, a water solution containing citric acid, the A-site cation precursor (barium oxide, Aldrich) and the active metal precursors (rhodium(II) acetate, Alfa Aesar; ruthenium acetate, Heraeus; tetraammineplatinum(II) hydroxide hydrate, Sigma-Aldrich) were added.
The resulting solution was neutralized with concentrated ammonium hydroxide and then slowly evaporated under vacuum to obtain a low density spongy material. The solid citrate precursor was crushed and sieved to obtain particles with dimension ranging from 150 to 300 μm, then the organic part was decomposed in a fixed bed reactor at 673 K with a N_2-O_2 mixture containing 2% of O_2 and calcined at 1123 K for 5 h to obtain the mixed oxide. The calcination temperature was chosen

according to the results reported by Viparelli et al. [21] showing that a calcination temperature of 1123 K gives rise to a better perovskite crystalline structure, in which the noble metal is well interspersed.
BET analysis of catalysts was performed using a Micrometrics ASAP 2000 V 2.05, in order to determine the surface area. The degree of crystallinity was estimated by X-ray diffraction (XRD). XRD patterns were obtained using an X-ray microdiffractometer, Rigaku D-max-RAPID, using Cu-Kα radiation. The lattice parameters were measured from XRD data using the software Match! based on Rietveld refinement. The XRD tests were performed also after a long term experimental dry reforming test to evaluate possible changes in the crystalline catalyst structure.
Temperature Programmed Reduction (TPR) measurements were performed in the laboratory apparatus described elsewhere [22]. A stream of 2%H_2 in N_2 (150 Ncm^3/min) was typically fed to the reactor loaded with 250 mg of catalyst with an heating rate of 10 K /min until 1273 K.
The rate of carbon deposition on the exhaust catalysts was measured through thermogravimetric analysis from T_{amb} to 1273 K (heating rate 10 K/min), that was performed in a thermogravimetric analyzer Q600, TA Instrument, coupled with PFEIFFER ThermoStar Quadrupole Mass Spectrometer.

2.2 Experimental set-up

The laboratory set-up, reported in Fig.1, is composed by a quartz tube reactor (di=0.8 cm, h=50 cm) equipped with a quartz frit for the formation of the catalyst bed made of 0.1 g of catalyst diluted in 2 g of silicon dioxide (grain size 0.1–0.3 mm) to minimize temperature gradients. The reactor was heated by an external cable heater controlled by a K-type thermocouple. The total inlet flow, composed by the reagents and N_2 to dilute the feed, was kept constant for all the performed tests at 0.6 l/min. This flow rate allows to approach the plug flow condition and to minimize the backmixing [23].
At the beginning of each test, the temperature was set to the desired reforming conditions and, once the operation conditions were reached, the feed flow was supplied.
At the reactor exit the water produced with the reverse water gas shift reaction was condensed and then the gas was sent to an online analyzer for the CO, CO_2 and CH_4 species (Simens Ultramat 23). The hydrogen concentration was determined discontinuously by gas chromatography (DANI 3800, carrier gas Argon) sampling the gas every 10 min.
For each catalyst different experimental tests varying the temperature were conducted in order to evaluate the performances of the catalysts and to obtain kinetic parameters. For each test, lasting 1 h, fresh catalyst was used. In order to evaluate the behavior of the perovskites varying the CO_2/CH_4 ratio, additional tests were performed at a temperature of 1023 K, keeping constant the total flow rate and varying only the molar fraction of the two reagents.
Experimental data were compared with the thermodynamic equilibrium conditions calculated with the minimization of Gibbs free energy considering that only the DRM and the RWGS reactions take place into the reactor.
The occurrence of deactivation was then evaluated performing long duration tests, lasted 60 h, at a fixed temperature (1023 K).
The operative conditions used in the experimental tests are reported in Table 1.

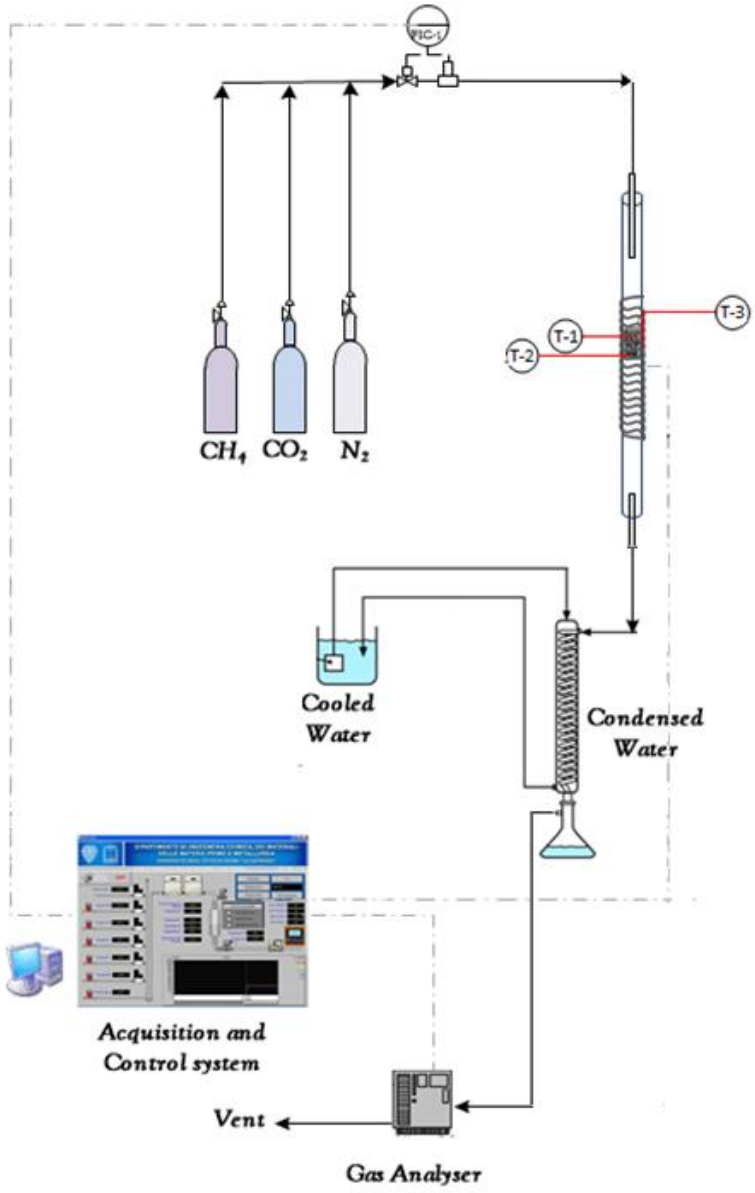

Fig. 1. Dry reforming experimental set-up.

Table 1: Operative conditions used in the experimental tests for the three catalysts.

T (K)	850-1150
Contact time (g_{cat} min l^{-1})	0.17
Inlet reagent flow (l min^{-1})	0.3
Inlet N_2 (l min^{-1})	0.3
CO_2:CH_4 (molar ratio)	0.8; 1.0; 1.2;1.4

2.3 Kinetic model

Based on the work of Wei and Iglesia [20], it was considered that dissociation of methane is the rate-determining step for DRM being the initial activation of C–H bond in CH_4 the kinetically limiting step. Indeed, the relevant forward rate constant for this process was observed to be the same with respect to a given metal, the metal dispersion, and the reaction conditions, being unaffected by the CO_2 concentration. Therefore under steady state conditions only one continuity equation is required for completely describing methane conversion, the mass balance for CH_4:

$$F_{CH_4,\text{in}} - F_{CH4,out} = (-r_n) \cdot w \tag{5}$$

Where *w* is catalyst weight [g].
Using eq. (5) it is possible to calculate the apparent reaction, or net reaction, rate of methane dry reforming expressed in units of [mol/(g s)].
In the absence of significant deactivation and variations of thermodynamic conditions and transport properties, forward reforming rates (r_f) can be rigorously obtained, employing the measured net reaction rates (r_n), using the equilibrium approach, by defining the β and η (the equilibrium factor) parameters from dry reforming thermodynamic reaction data, the thermodynamic equilibrium constant $K_{equilibrium\ \mathrm{DR}}$ and the partial pressure quotient K_{DR} being the ratio between the measured products and reagents partial pressures [Pi] raised to the stoichiometric coefficients[24]:

$$\beta = 1 - \eta_{DR} \tag{6}$$

$$\eta_{DR} = \frac{K_{DR}}{K_{equilibrium,\,DR}} \tag{7}$$

$$K_{DR} = \frac{P_{CO^2} \cdot P_{H_2^2}}{P_{CH_4} \cdot P_{CO_2}} \tag{8}$$

$$K_{equilibrium\ \mathrm{DR}} = \exp\left(\frac{-\Delta G°(T)}{RT}\right) \tag{9}$$

$$r_f = \frac{r_n}{\beta} \tag{10}$$

The determination of the dependencies of the forward reaction rate is based on the work of Wei and Iglesia, which reported that the reaction rate is proportional to the CH_4 partial pressure and independent on co-reactants partial pressures, concluding that only the C-H bond activation steps are kinetically relevant. As a consequence, forward rate is not dependent on CO and H_2 concentrations and thus CH_4 dry reforming rate become simply first order in CH_4 and zero order in CO_2[20]:

$$r_f = K \cdot P_{CH_4} \tag{11}$$

Additional effects due to the concentrations of the products are taken into account in the evaluation of the parameter β.

Kinetic parameters of the dry reforming, activation energy Ea and pre-exponential factor, can be carried out with the Arrhenius law linearizing the equation and taking into account data at different temperatures.
In addition to the dry reforming reaction, also the reverse reaction of water gas shift takes place but it is not possible to calculate its reaction rate because, under the operating conditions, it is at equilibrium [11].

3. Results and discussion

3.1 Characterization of fresh catalysts

The results of the physical characterization of the catalysts are reported in Table 2. The BET specific surface of the three perovskites are consistent with the values reported in the literature for perovskite obtained with the citrate method (6-13 m^2/g) [21].
Looking at the results of the XRD analysis reported in Fig. 2 it can be noticed that the prevailing signals are those corresponding to the perovskite $BaZrO_3$, meaning that $BaCO_3$ is present only in very low amount. Comparing the peaks concerning the $BaZrO_3$ and those obtained from the analysis of $BaZrRuO_3$, $BaZrRhO_3$ and $BaZrPtO_3$ it is evident that the same perovskite structure is present. The effect of the metal loading is almost not visible, except for a very small shift of the peaks in the XRD curves. The metal loadings is in fact too low (5 % wt.) to be detected by XRD. This behavior was expected as reported by Viparelli et al. [21], which observed a small shift in XRD only at high noble metal loadings (18.6 wt%) for the same perovskites. Furthermore the presence of phases that can be attributed to the segregation of transition metals can be excluded looking at the XRD results, meaning that the transition metals are well inserted in the crystal structure and strongly held inside a crystalline structure. The cell parameters are reported in Table 2, the good agreement of experimental with calculated spectra confirms that the cell is cubic.

Table 2: Main physical proprieties of catalysts.

	surface area (m^2/g)	Pore volume (cm^3/g)	Particle size (μm)	Cell parameter (Å)
$BaZrO_3$	8.4	-	-	-
$BaZrRhO_3$	11.7	0.05	<150	4.16219
$BaZrRuO_3$	12.8	0.07	<150	4.13607
$BaZrPtO_3$	10.3	n.d.	<150	4.14945

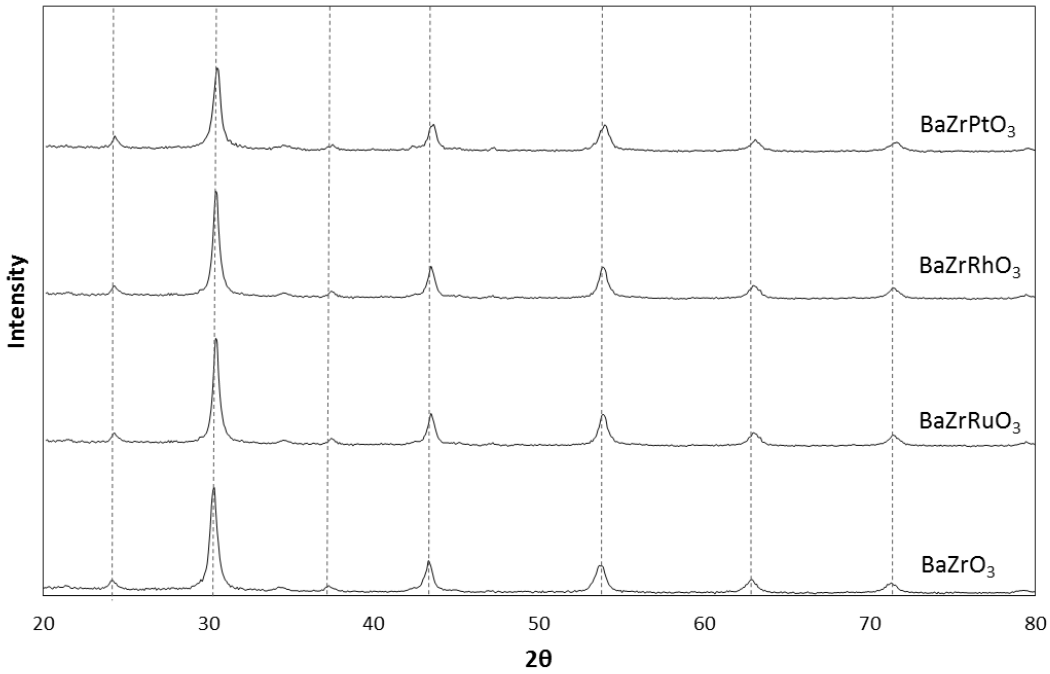

Fig.2. X-ray diffraction (XRD) patterns for the three catalyst samples compared with the XRD pattern of the $BaZrO_3$ perovskite structure.

TPR experiments were performed on the fresh catalysts in order to study the reduction behavior of the oxidized phases. Additionally, measurements on the $BaZrO_3$ perovskite were also carried out.
The H_2 uptake profiles after deconvolution, recorded over the three catalysts as well as the bare support, are displayed in Fig.3. The low temperatures peaks (448 and 444 K, respectively), observed over both $BaZrRhO_3$ and $BaZrRuO_3$ samples, are assigned to the presence of highly reducible metals-containing sites [25,26]. However, the H_2 uptakes ascribable to the low temperature peaks are significantly different for the latter two samples: in the case of Rh containing catalyst, the consumption was equal to 1109 $\mu molH_2/g_{cat}$ while a lower value (Table 3, 89 $\mu molH_2/g_{cat}$) was recorded for the $BaZrRuO_3$ catalyst. Moreover, Ru and Pt based catalysts displayed reduction peaks at higher temperatures (586 and 614 K, respectively) which are also ascribable to the reduction of noble metals oxides to their metallic form.
All the samples showed a broad peak between 700 and 950 K, which is probably due to the reduction of the oxygen species on the perovskite surface or lattices [27]. Furthermore, over the catalysts containing Rh and Pt it is also possible to observe a broad peak at T > 1000 K, which is indicative of the reduction of bulk oxygen [28]. Conversely, a very small H_2 uptake was globally observed between 630 and 1180 K over the $BaZrO_3$ perovskite. However, the increase of the support reducibility following the substitution with a noble metal as well as the appearance of reduction peak at low temperatures was previously reported for perovskite samples [29].
$BaZrRhO_3$ catalyst showed the highest reducibility: the total H_2 uptake (2099 $\mu molH_2/g_{cat}$) was almost twice the theoretical one (971 $\mu molH_2/g_{cat}$). In fact, hydrogen spillover phenomena [30,31], commonly promoted by noble metals, favor the migration of H_2 from the just reduced metal particles to the support, thus resulting in experimental uptake higher than the expected values. Also in the case of Ru containing sample, the experimental uptake is slightly higher than expected value while for the $BaZrPtO_3$ catalyst the calculated consumption is lower.
The better catalytic activity of the samples containing Rh and Ru, described in the following section, can be linked to their higher reducible nature [32] with respect to $BaZrPtO_3$ catalyst. In fact, the oxygen vacancies, caused by the partial B-site-ion substitution, may serve as active sites for CO_2 dissociation into gas phase CO and surface oxygen species [33].

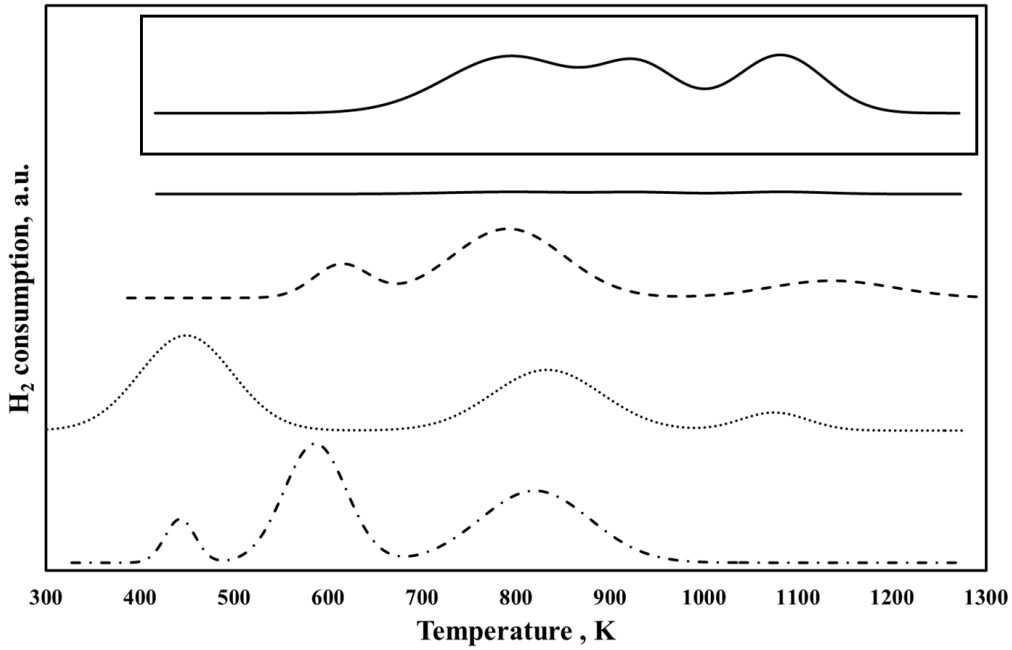

Fig. 3. H_2 consumption profile for $BaZrRuO_3$ (dashed point line), $BaZrRhO_3$ (point line), $BaZrPtO_3$ (dashed line), $BaZrO_3$ (continuous line); the insertion shows a magnification of the bare support profile.

In addition, the presence of active oxygen species favors the oxidation of coke precursors, thus enhancing the resistance towards coke formation.

Table 3. Quantitative results of H_2-TPR analysis of fresh catalyst samples

	T (K)	Experimental ($\mu mol/g_{cat}$)	Total experimental ($\mu mol/g_{cat}$)	Total expected ($\mu mol/g_{cat}$)
$BaZrO_3$	795	15	32	
	933	7		
	1079	10		
$BaZrRhO_3$	448	1109	2099	971
	833	836		
	1075	154		
$BaZrRuO_3$	444	89	1012	972
	586	473		
	820	450		
$BaZrPtO_3$	614	70	472	524
	792	301		
	1135	101		

3.2 Dry reforming experimental results

In Fig.4 the comparison between the results of the tests performed at different temperatures for the three catalysts is reported. The methane and carbon dioxide conversions were calculated as:

$$X_i = \frac{V_i^{in} - V_i^{out}}{V_i^{in}} \quad (12)$$

where V^i_{in} and V^i_{out} are the volumetric flow rates of the species i in the feeding flow and in the flow exiting from the reactor, respectively. The CO and H_2 yields were calculated as:

$$Y_{CO} = \frac{V_{CO}^{out}}{V_{CH4}^{in}+V_{CO2}^{in}} \quad (13)$$

$$Y_{H2} = \frac{V_{H2}^{out}}{2\,V_{CH4}^{in}} \quad (14)$$

The perovskite with rhodium presents the highest activity: CH_4 and CO_2 conversions are about 95 % at 1150 K. At 1050 K the conversions and yields reach the thermodynamic equilibrium values. This result suggests that it would be possible to work with lower catalyst quantity, obtaining the same results.

The Pt catalyst shows the lowest activity; as it can be noticed from the Fig.4a, temperatures higher than 923 K are needed to obtain an increase in the reagent conversions, suggesting that for lower temperature the catalyst is out from the temperature interval for which it is active.

The Ru perovskite has an intermediate behavior between Rh and Pt catalysts, approaching the thermodynamic equilibrium at the maximum tested temperature.

As shown in Fig.4a and Fig.4b, for the Pt and Ru perovskites the CH_4 conversion is always lower than the CO_2 one. This behavior is attributed to the occurring of the reverse water gas shift reaction that leads to a major conversion of the CO_2. For the Rh catalyst, instead, the two species present almost the same conversion values as indicated by the stoichiometry of the DRM reaction. In this condition, in fact, CO_2 reacts mainly with CH_4 due to the higher activity of the Rh perovskite in the DRM process. The influence of RWGS is, thus, minimized, leading to a higher concentration of H_2 exiting from the reactor. These results are confirmed by the H_2/CO ratio values (Fig.5) that for the Rh catalysts approach 1 at temperature 1100 K.

a)

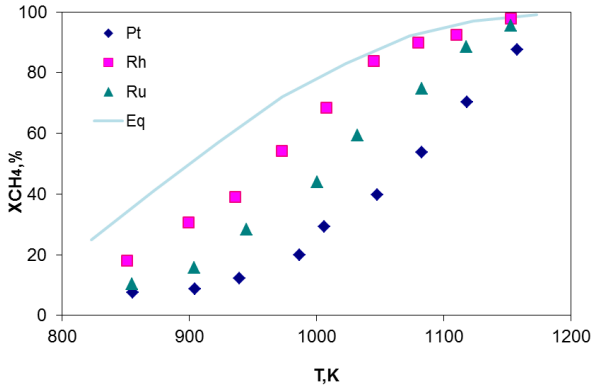

b)

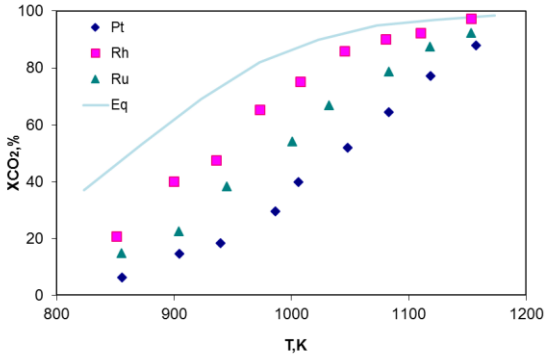

c)

d)

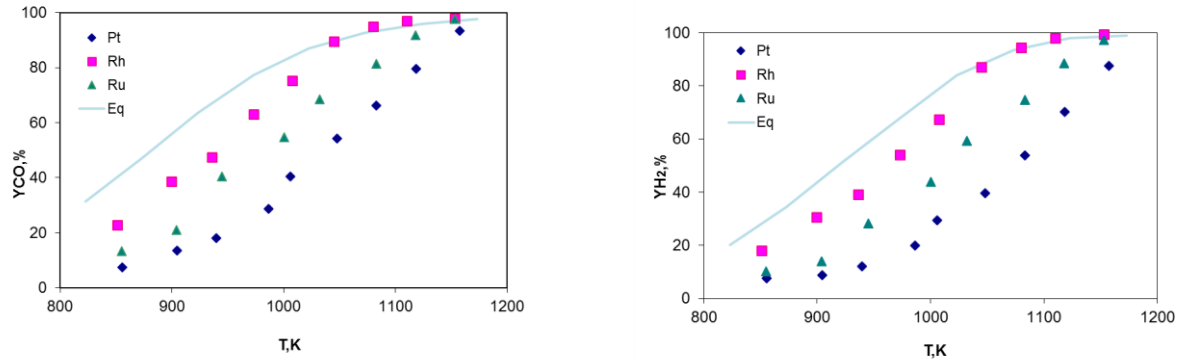

Fig.4. Results of the dry reforming tests at different temperatures and CO_2/CH_4=1; a) CH_4 conversion, b) CO_2 conversion, c) CO yield and d) H_2 yield.

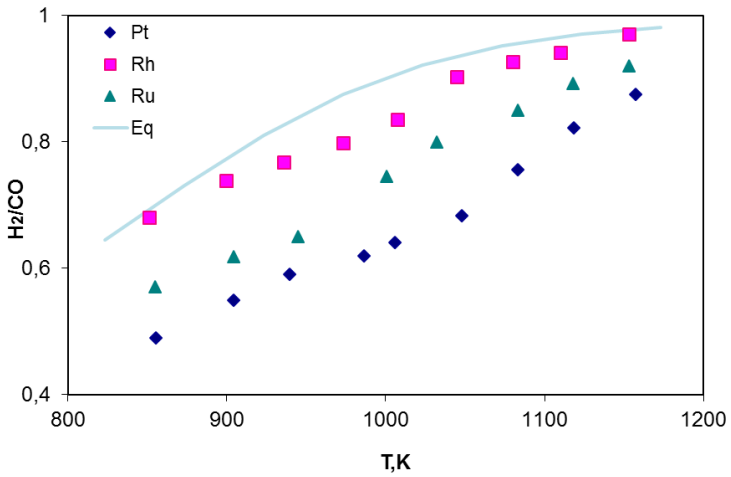

Fig.5. H_2/CO ratio obtained with the dry reforming tests.

The trend of CH_4 conversion as function of CO_2/CH_4 molar ratio for catalyst temperature of 1023 K is shown in Fig.6a, where the theoretical equilibrium values at the same conditions are also reported. As expected, an increase of the methane conversion is obtained raising the molar concentration of CO_2 in the feed flow rate. The H_2/CO ratio (Fig.6b) presents the opposite behavior of the CH_4 conversion, the decrease of the H_2/CO ratio is due to the occurring of the reverse water gas shift reaction for higher CO_2 concentration.

a) b)

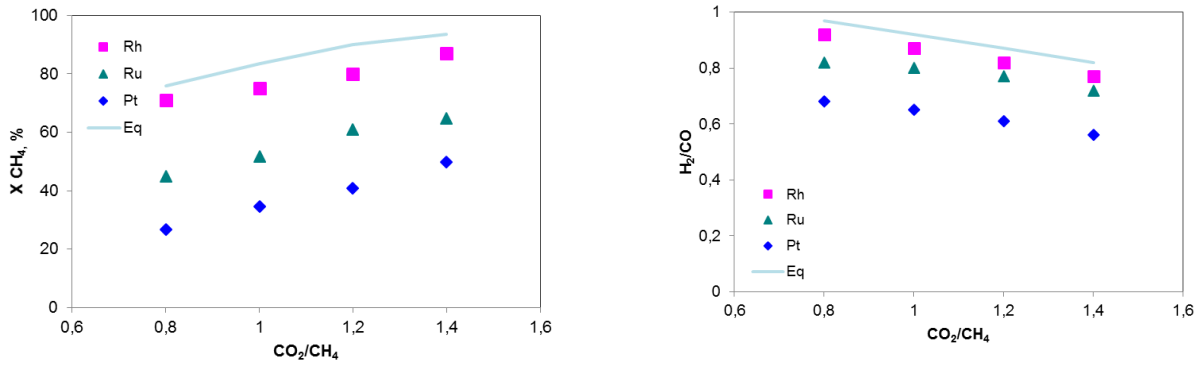

Fig.6. CH_4 conversion and H_2/CO ratio for the three catalysts obtained from experimental tests performed at different CO_2/CH_4 ratios at 1023 K.

The long duration tests, reported in Fig.7, show that the Rh and Ru perovskites do not deactivate while the Pt perovskite presents a slight loss of activity that was measured to be about 10 % after 65 h. These results were expected looking at the XRD analysis of the Rh perovskite samples before and after the tests (Fig.3) where no difference in the peak amplitude were detected.

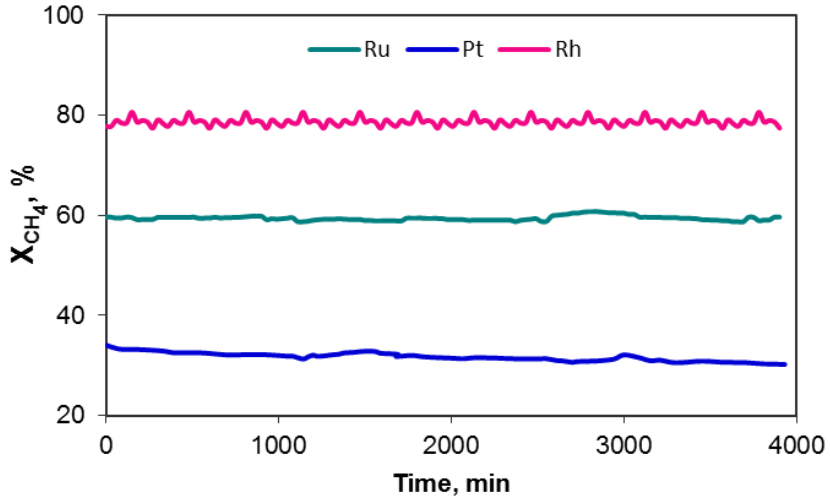

Fig.7. CH_4 conversion obtained for the three catalysts in long duration tests of 65 h at 1023 K and for CO_2/CH_4=1.

3.3 *Characterization of exhausts catalysts*

The comparison between the XRD analysis of the $BaZrRhO_3$ perovskite before and after the experimental DRM tests is reported in Fig.8, showing a good stability of the perovskite structure; the same applies for the other catalysts. In fact, no significant difference can be detected in the peak amplitude of the two samples and in lattice parameters that present the same values of the fresh catalysts.

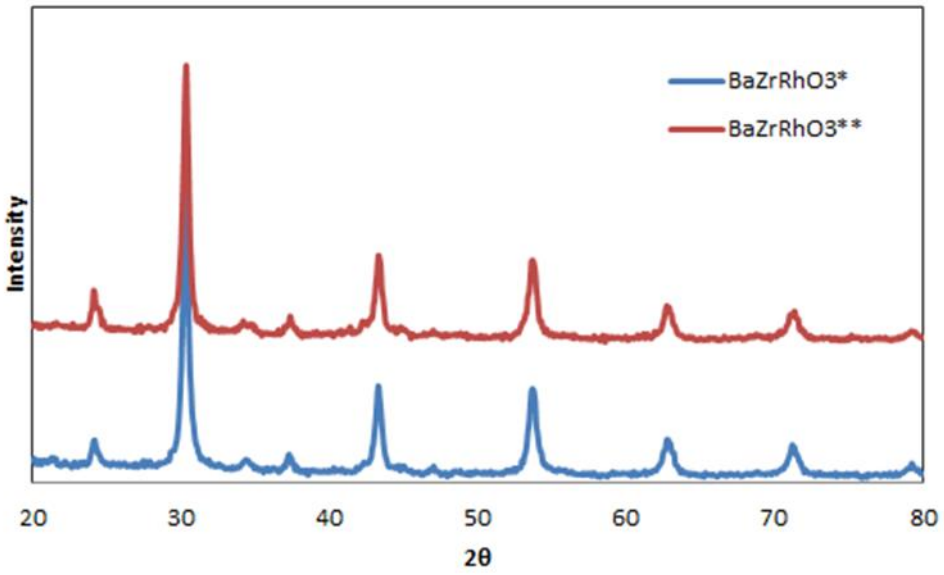

Fig.8. XRD of the $BaZrRhO_3$ perovskite before (*) and after (**) DRM tests.

Pt, Rh and Ru perovskites were characterized through thermogravimetric (TG) analysis in order to estimate the carbon formation rate (C, Eq.15), defined as the mass of carbon (m_{coke}) formed per gram of catalyst (m_{cat}), normalized with respect to the time-on-stream (TOS):

$$C = \frac{m_{coke}}{m_{cat} * TOS} \tag{15}$$

The results in terms of TG and mass spectrometry recorded over $BaZrRhO_3$ catalyst post stability tests are shown in Fig.9. It's worthwhile noting that, besides water, the only signal which underwent variations in the mass spectrum is related to the mass 44 (CO_2). The weight variation (Fig. 9 (a)) observed at T< 470 K is ascribable to water release from catalyst surface. Conversely, the increase of CO_2 signal (Fig. 9 (b)) attested that the weight loss recorded at T>520 K can be attributed to coke oxidation reaction. On the basis of this analysis, carbon formation rate was calculated for the three perovskites and the results are summarized in Table 4.

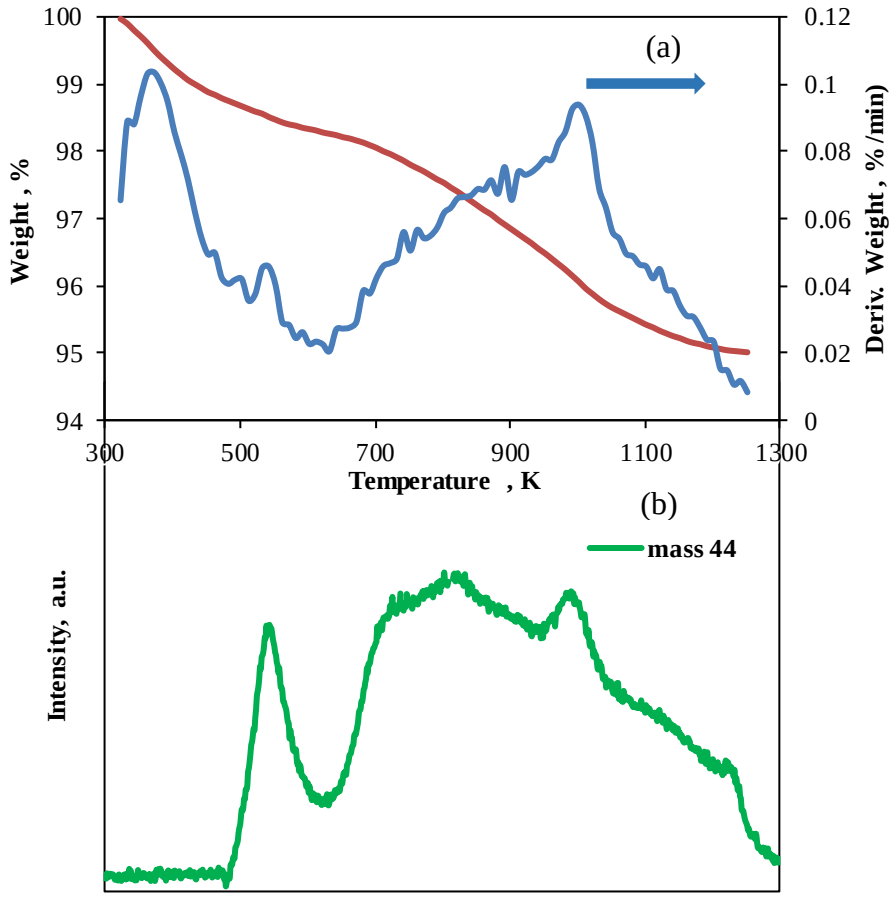

Fig. 9. TG (a) and mass spectrometry (b) on Rh perovskite after stability test.

Table 4: Carbon formation rates calculated through thermogravimetric analysis.

	C ($g_{coke}/(g_{cat}*h)$)
$BaZrRhO_3$	0.0019
$BaZrRuO_3$	0.0027
$BaZrPtO_3$	0.0094

The lowest carbon deposition rate was observed over the Rh perovskite, which also showed the most promising results during stability tests (Fig.7). However, $BaZrRuO_3$ catalyst displayed a coke selectivity very similar to the value recorded over $BaZrRhO_3$, which, despite reached a lower CH_4 conversion, assured a stable behavior during time-on-stream. On the contrary, a significant carbon formation rate value was recorded over the $BaZrPtO_3$ sample, which displayed a loss of activity of almost 10%.

The results of stability tests over $BaZrRhO_3$ catalyst, in terms of carbon formation rate, were compared with the data presented in the recent literature (Table 5), finding that lower values reported in other papers were obtained after TOS performed in conditions more advantageous (higher contact times and/or higher temperatures, which should thermodynamically favor dry reforming of methane instead of carbon deposition [34]), compared to the operating parameters employed in this work. It is also interesting to note that space velocities (GHSV) higher than that of the present work are rarely found in other works. These observations make even more promising and competitive the performances of $BaZrRhO_3$ catalyst.

Table 5: Comparison between the coke formation rates obtained with Rh perovskite and the values reported in the recent literature; all the stability tests were carried out at atmospheric pressure.

Sample	Ref.	C ($g_{coke}/(g_{cat}*h)$)	GHSV (h^{-1})	Tests Conditions
$Ni@SiO_2$	[35]	0.00049	48000	T=1023 K CO_2/CH_4=1
$NiB(0.5)/\gamma Al_2O_3$	[36]	0.0012	30000	T=973 K CO_2/CH_4=1
La-NiMgAlO	[37]	0.0014	4800	T=923 K CO_2/CH_4=1
$LaNi_{0.8}Zn_{0.2}O_3$	[38]	0.0093	300000	T=1023 K CO_2/CH_4=1
La_2NiO_4/KIT-6	[39]	0.052	33600	T=1073 K CO_2/CH_4=1.1
Ni-CaO-ZrO_2	[40]	0.00067	79000	T=1123 K CO_2/CH_4=1.2
$Na_{0.5}La_{0.5}Ni_{0.3}Al_{0.7}O_{2.5}$-$CeO_2ZrO_2$	[41]	0.032	30000	T=1153 K CO_2/CH_4=1
10Ni/CZ/SBA-15	[42]	0.0011	20000	T=873 K CH_4/CO_2=1
Ni/32.4$BaTiO_3$-Al_2O_3	[43]	0.0070	24000	T=963 K CO_2/CH_4=1
10.7Ni/CeO_2-Al_2O_3	[44]	0.0125	90000	T=873 K CO_2/CH_4=1
Ni_{15}CeMgAl	[45]	0.010	48000	T=1023 K CO_2/CH_4=1.04
$BaZr_{0.8649}Rh_{0.1351}O_3$	This work	0.0019	353000	T=1023 K CH_4/CO_2=1

3.3 Kinetic study

The trends of the forward reaction rates of the three catalysts, reported in Fig.10, are in accordance with the experimental results obtained. In Fig.11 the Arrhenius plots are shown, the model completely fits the experimental data, allowing to calculate activation energies and pre-exponential values. The resulting average values of the kinetic parameters for the three perovskite catalysts are reported in Table 6.

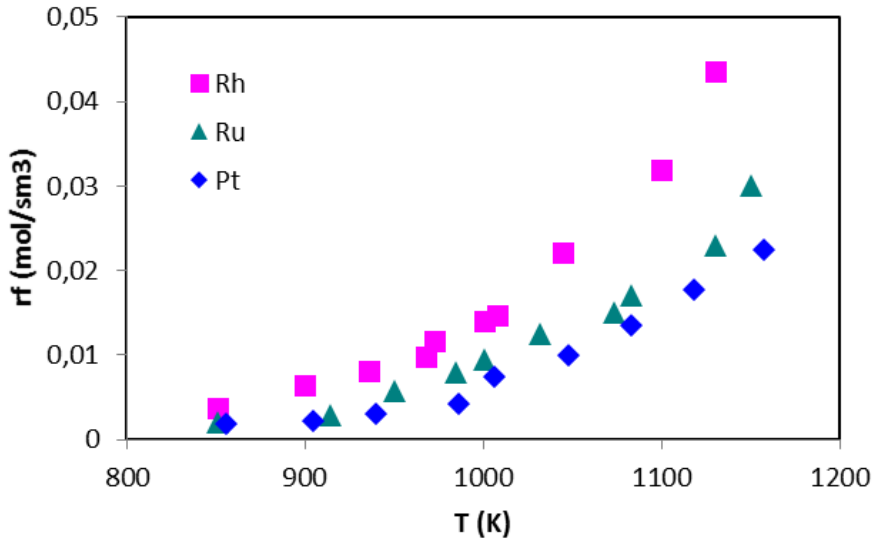

Fig.10. Forward reaction rates calculated for the three perovskites.

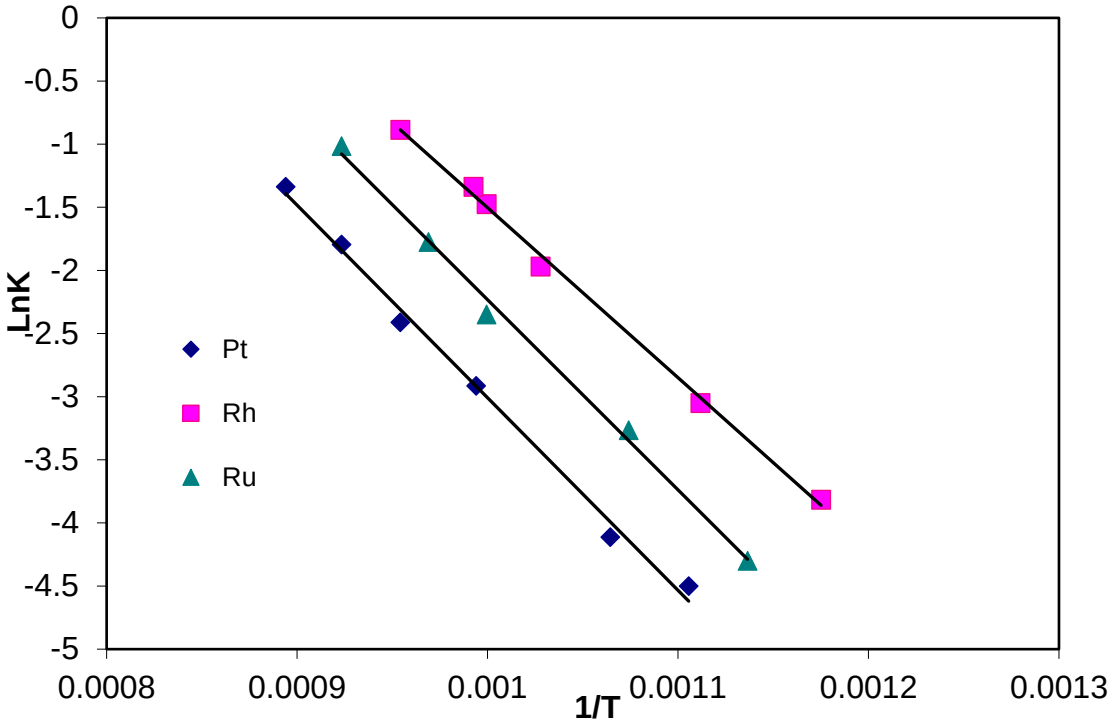

Fig.11. Arrhenius plot for the three catalysts

To calculate the kinetic parameters, only the experimental data obtained in the temperature interval 923-1050 K were taken into consideration. The temperature of 923 K corresponds to the Pt perovskite activation temperature and the 1050 K value is the temperature at which the equilibrium is reached with Rh perovskite.

The values of the activation energies confirm the results obtained in the experimental tests. The Rh perovskite has the lowest activation energy and the Pt one the highest. These results are in accordance with literature data for catalysts having the same active species [46,47].

Table 6: Calculated average value of activation energy and pre-exponential factor obtained for the three catalysts.

	E (kJ mol^{-1})	A (mol $g_{cat}^{-1}s^{-1}atm^{-1}$)
Rh	111.9 ± 6	156007
Ru	128.6 ± 4	532852
Pt	133.8 ± 6	504841

4. Conclusions

In this study the performances of three ternary perovskite type oxides $BaZr_{(1-x)}Me_xO_3$ using noble metals Rh, Ru and Pt as active species and produced with the modified citrate method were investigated in the DRM process. The experimental tests pointed out that the activity of the catalysts increases with the active species as: Pt<Ru<Rh. It is also demonstrated that the Pt shows a very low activity for temperature lower than 923 K. The better catalytic activity of the samples containing Rh and Ru, as demonstrated by the TPR test, can be linked to their high reducible nature. No deactivation of the Rh and Ru catalysts is detected from the long duration tests, while a slight loss of activity is measured when Pt perovskite is used, due to a significant carbon formation rate over the $BaZrPtO_3$ sample.
The model used for the calculation of the kinetic parameters has demonstrated to be adequate in the interpretation of the experimental results, giving values of the activation energy that confirm the experimental results.
It is also interesting to note that notwithstanding the high space velocities (GHSV) and the low temperatures used in this work, the carbon formation rate of $BaZrRhO_3$ catalyst is limited if compared with literature data obtained with more favorable operative conditions, making even more promising and competitive the performances of this catalyst.

References

[1] M.C.J. Bradford, M.A.Vannice, Catal. Rev. Sci. Eng. 41 (1999) 1-42.
[2] X.E. Verykios, Int. J. Hydrogen Energ. 28 (2003) 1045-1063.
[3] M.Usman, W.M.A.W. Dau, H.F. Abbas, Renew. Sust. Energ. Rev. 45 (2015) 710-744.
[4] J.D. Holladay, J. Hu, D.L. King, Y. Wang, Catal. Today 139 (2009) 244–260.
[5] M.S. Fan, A.Z. Abdullah, S. Bhatia, ChemCatChem 1 (2009) 192-208.
[6] M. Stelmachowski, L. Nowicki, Appl. Energy 74 (2003) 85-93.
[7] J.R.H. Ross, A.N.J. van Keulen, M.E.S. Hegarty, K. Seshan, Catal. Today 30 (1996) 193-199.
[8] D.J. Wilhelm, D.R. Simbeck, A.D. Karp, R.L. Dickenson, Proc. Technol. 71 (2001) 139-148.
[9] C.S. Lau, A. Tsolakis, M.L. Wyszynski, Int. J. Hydrogen Energ. 36 (2011) 397-404.
[10] M.F. Demirbas, M. Balat, H. Balat, Energy Convers. Manag. 52 (2011) 1815-1828.
[11] J.R. Rostrup-Nielsen, J.H.B. Hansen, J. Catal. 144 (1993) 38–49.
[12] M.E. Rivas, J.L.G. Fierro, M.R. Goldwasser,E. Pietri, M.J. Perez-Zurita, A. Griboval-Constant, G. Leclercq Appl. Catal. A 344 (2008) 10–19
[13] E. Yang, Y. Noh, S. Ramesh, S. S. Lim, D. J. Moon Fuel Process. Technol.134 (2015) 404-413
[14] G. Valderrama, A. Kiennemann, M.R. Goldwasser, J. Power Sources 195 (2010) 1765-1771.
[15] G.S. Gallego, C. Batiot-Dupeyrat, J. Barrault, E. Florez, F. Mondragon, Appl. Catal. A 334 (2008) 251-258.
[16] M.A. Pena, J.L.G. Fierro, Chem. Rev. 101 (2001) 1981-2017.

[17] P.L.Villa, Solid solutions, applicable as catalysts, with a perovskite structure comprising noble metals, PCT/EP02/07906 on the 17.07.02 and USA Patent no. 7,166,267 (granted 23.01.07), European Patent Application (filed on 16.07.04).
[18] G. Taglieri, G. Tersigni, P.L. Villa, C. Mondelli, Int. J. Inorg. Mater. 1 (1999) 103-110.
[19] P.G. Sundell, M.E. Bjorketun, G. Wahnstrom, Phys. Rev. B 73 (2006) 104-112.
[20] J. Wei, E. Iglesia, J. Catal. 225 (2004) 116-127.
[21] P. Viparelli, P. Villa, F. Basile, F. Trifirò, A. Vaccari, P. Nanni, M. Viviani, Appl. Catal. A 280 (2005) 225-232.
[22] V. Palma, M. Miccio, A. Ricca, E. Meloni, P. Ciambelli, Fuel 138 (2014) 80–90.
[23] J. Xu, G.F. Froment, AIChE J. 35 (1989) 88–96.
[24] M. Maestri, D.G. Vlachos, A. Beretta, G. Groppi, E. Tronconi, J. Catal. 259 (2008) 211-222.
[25] P. Ammendola, L. Lisi, B. Piriou, G. Ruoppolo, Chem. Eng. J., 154 (2009) 361-368.
[26] Y. Wu, C. Dujardin, C. Lancelot, J.P. Dacquin, V.I. Parvulescu,, M. Cabié, C.R. Henry, T. Neisius, P. Granger, J. Catal. 328 (2015) 236-247.
[27] Z. Wang, B. Liu, J. Lin, Applied Catalysis A: General 458 (2013) 130–136.
[28] A. Bampenrat, V. Meeyoo, B. Kitiyanan, P. Rangsunvigit, T. Rirksomboon, Appl. Catal. A: Gen. 373 (2010) 154–159.
[29] G.C.Mondragón Rodríguez, Y. Gönüllü, D. Ferri, A. Eyssler, E. Otal, B. Saruhan, Mater. Res. Bul. 61 (2015) 130-135.
[30] N. Mota, R.M. Navarro, M.C. Alvarez-Galvan, S.M. Al-Zahrani, J.L.G. Fierro, J. Power Sources 196 (2011) 9087-9095.
[31] C.-L. Li, Y.-C. Lin, Appl. Catal. B: Environ. 107 (2011) 284-293.
[32] M. H. Amin, S. Putla, S. B. A. Hamid, S. K. Bhargava, Appl. Catal. A: Gen. 492 (2015) 160–168.
[33] S. Gaur, D. J. Haynes, J. J. Spivey, Appl. Catal. A: Gen. 403 (2011) 142–151.
[34] T.D. Gould, A. Izar, A.W. Weimer, J.L. Falconer, J.W. Medlin, ACS Catal. 4 (2014) 2714–2717
[35] J. Zhang, F. Li, Appl. Catal B: Environ. 176–177 (2015) 513–521.
[36] A. Fouskas, M. Kollia, A. Kambolis, Ch. Papadopoulou, H. Matralis, App. Catal. A: Gen. 472 (2014) 125-134.
[37] A. Serrano-Lotina, L. Daza, Appl. Catal A: Gen. 474 (2014) 107-113.
[38] G.R. Moradi, M. Rahmanzadeh, F. Khosravian, J. CO_2 Util. 6 (2014) 7-11.
[39] Y.H. Guo , C. Xia , B.S. Liu, Chem. Eng. J., 237 (2014) 421–429.
[40] Q.J. Chen, J. Zhang, Q.W. Jin, B.R. Pan, W.B. Kong, T. J. Zhao, Y.H. Sun, Catal. Today. 215 (2013) 251–259.
[41] M. N. Pérez-Camacho, J. Abu-Dahrieh, A. Goguet, K. Sun, D. Rooney, Chinese J Catal. 35 (2014) 1337-1346.
[42] A. Albarazi, P. Beaunier, P. Da Costa, Int. J. Hydrogen Energ., 38 (2013) 127-139.
[43] X. Li, Q. Hu, Y. Yang, Y. Wang, F. He, Appl. Catal. A: Gen. 413-414 (2012) 163-169.
[44] I. Luisetto, S. Tuti, C. Battocchio, S. Lo Mastro, A. Sodo, Appl. Catal. A: Gen. 500 (2015) 12-22.
[45] Z. Bao, Y. Lu, J. Han, Y. Li, F. Yu, Appl. Catal A:Gen. 491 (2015) 116-126.
[46] J.G. Jacobsen, T.L. Jorgensen, I. Chorkendorff, J. Sehested, Appl. Catal. A 377 (2010) 158-166.
[47] J.F. Munera, S. Irusta, L.M. Cornaglia, E.A. Lombardo, D.V. Cesar, M. Schmal, J. Catal. 245 (2007) 25-34.